Journal of Atmospheric and Solar-Terrestrial Physics 179 (2018) 69–80

Contents lists available at ScienceDirect

Journal of Atmospheric and Solar-Terrestrial Physics

journal homepage: www.elsevier.com/locate/jastp

Near-global GPS-derived PWV and its analysis in the El Niño event of 2014–2016

Qingzhi Zhao[a,*], Yibin Yao[b], Wan Qiang Yao[a], Zufeng Li[c]

[a] College of Geomatics, Xi'an University of Science and Technology, Xi'an, China
[b] School of Geodesy and Geomatics, Wuhan University, Wuhan, China
[c] Powerchina Northwest Engineering Corporation Limited, Xi'an, China

ARTICLE INFO

Keywords:
ZTD
PWV
Radiosonde
IGS

ABSTRACT

Precipitable water vapour (PWV) is a key factor in activities related to climate monitoring and the global hydrologic cycle. In this paper, the PWV time series with an accuracy of about 1.3 mm is obtained on a global scale using the zenith total delay (ZTD) derived from International GNSS Service (IGS). A theoretical error formula from ZTD to PWV reveals that the PWV error induced by errors in ZTD, surface pressure (P_s) and weighted mean temperature (T_m) is about 1–1.5 mm. P_s and T_m are two key factors during the conversion of ZTD to PWV, which can be derived from the Global Geodetic Observing System (GGOS) Atmosphere. The GPS-derived and radiosonde-derived PWV time series are compared at 97 collocated stations on a global scale, which shows the maximum/minimum/mean root mean square (RMS) errors and Bias of 1.8/0.6/1.3 mm and 2.6/2.9/4.0/5.2 mm, respectively with a data utilisation rate of 96.8%. By analysing the periodograms of GPS-derived PWV time series using the Lomb-Scargle method, preliminary result shows the various oscillations characteristics of PWV time series at different stations. Finally, the diurnal variations of PWV time series during the El Niño event of 2014–2016 are analysed and revealed an interesting climate signal.

1. Introduction

Atmospheric water vapour is one of the most important factors influencing the atmospheric radiation, thermodynamics and hydrological cycles. The integral of water vapour through the vertical depth of the troposphere is commonly known as the precipitable water vapour (PWV), which can be estimated based on the Global Positioning System (GPS) technique and used to reflect the water vapour circulation and global climate change (Bevis et al., 1992; Wang et al., 2007; Jin and Luo, 2009; Baldysz et al., 2015). Traditionally, radio-sounding (sounding balloon) and satellite measurement (infrared sounders and microwave radiometers) are two main methods used to detect the atmospheric water vapour and study the water vapour climatology (Gaffen et al., 1991; Ross and Elliott, 1996, 2001; Gao et al., 2004; Trenberth et al., 2005), but such methods are still restricted by the quality of radiosonde data and a lack of high spatio-temporal resolution observations.

Since Bevis et al. (1992) first proposed a method to obtain PWV, the GPS has been widely applied in the field of meteorology with its superiority of a high spatio-temporal resolution as well as a low cost (Tregoning et al., 1998; Hernández-Pajares et al., 2001; Basili et al., 2004; Nilsson and Gradinarsky, 2006; Jin et al., 2007). The accuracy of PWV has been validated with independent data from other instruments, such as radiosondes, satellite radiometer soundings and microwave data. The above results demonstrate that the PWV derived from GPS observations can reach the same accuracy as conventional methods with an RMS error of 1–2 mm (Elgered et al., 1997; Niell et al., 2001; Adams et al., 2011; Grejner-Brzezinska, 2013). Therefore, the GPS-derived PWV has a substantial potential in meteorological studies, such as improving the ability of numerical weather predictions and obtaining diurnal PWV variations (Kuo et al., 1993; Dai et al., 2002; Wu et al., 2003). Unfortunately, the International GNSS Service (IGS) only provides the ZTD products while the PWV time series is not available due to the lack of collocated surface meteorological observations. Even the meteorological data for some collocated stations is available, the data quality is poor and noisy (Wang et al., 2007; Jin and Luo, 2009). Usually, the surface meteorological parameters used for converting ZTD to PWV at GPS stations are interpolated from the National Center for Environment Prediction/National Center for Atmospheric Research (NCEP/NCAR) (Wang et al., 2007), European Center for Medium-Range Weather Forecasts (ECMWF) ERA-Interim global reanalysis products (Wang et al., 2016; Baldysz et al., 2018) or global surface synoptic

* Corresponding author.
E-mail address: zhaoqingzhia@163.com (Q. Zhao).

https://doi.org/10.1016/j.jastp.2018.06.016
Received 27 April 2018; Received in revised form 28 June 2018; Accepted 28 June 2018
Available online 30 June 2018
1364-6826/

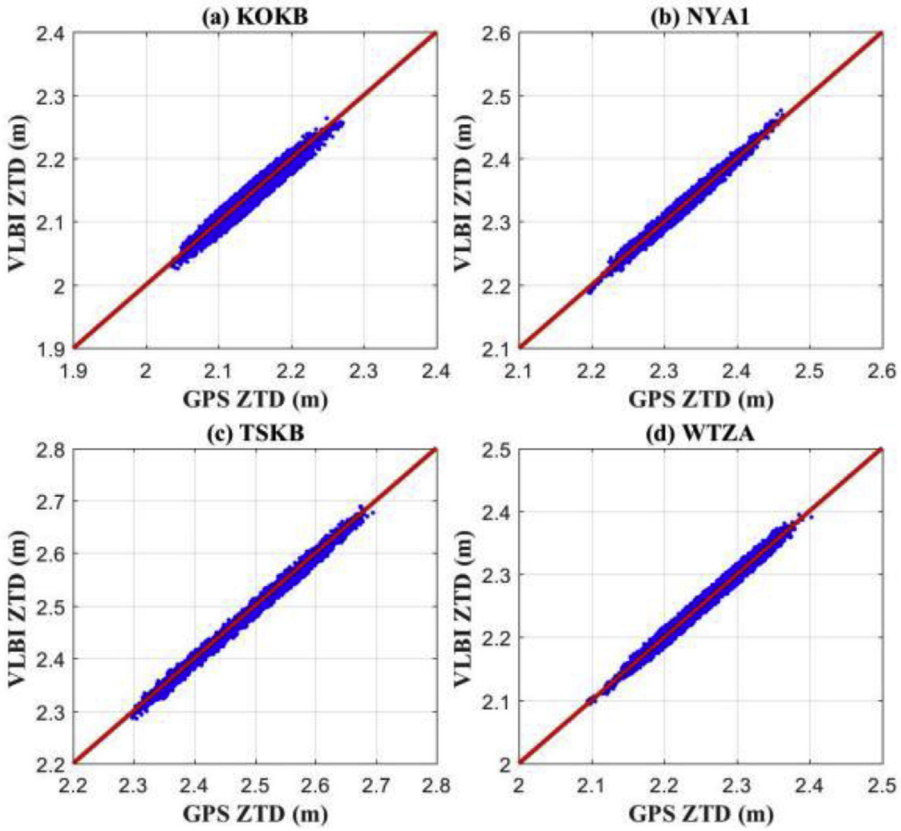

Fig. 1. Comparison of GPS-derived and VLBI-derived ZTD at four collocated stations, (a) KOKB, (b) NYA1, (c) TSKB and (d) WTZA over the period of 2002–2015.

observations (Jin and Luo, 2009). Schueler et al. (2001) has derived a PWV dataset on a global scale using interpolated meteorological parameters at specific GPS stations from various numerical weather model reanalysis products. The results from Schueler et al. (2001) indicates that GPS water vapour estimation without any direct use of numerical weather models or radiosonde data is possible up to a satisfactory degree of accuracy. Wang et al. (2007) proposed a method for obtaining PWV products from the IGS network with an RMS error less than 3 mm over the period of 1997–2004 by using the three-hourly surface measured data interpolated to GPS sites from about 15,000 global stations; in addition, the result of this study also illustrates the value of GPS-derived PWV for examining the quality of other data sets, such as those from radiosondes and numerical weather prediction (MWP).

Here, a long time-series of PWV products with the time interval of 2 h on a global scale is retrieved from the IGS GPS network by combing the corresponding meteorological parameters provided by Global Geodetic Observing System (GGOS) Atmosphere. The validations of the ZTD products derived from the IGS with 4, 94 and 269 stations, respectively are first performed by comparing with the independent Very Long Baseline Interferometry (VLBI) and radio sounding techniques as well as the data from GGOS atmosphere in Section 2. In Section 3, the theoretical error formula from ZTD to PWV is analysed and a comparison between GPS-derived and radiosonde-derived PWV at 97 collocated stations is performed over the period of 2005–2016. Annual, semi-annual and seasonal-annual oscillations of PWV are analysed by introducing the Lomb-Scargle periodogram method and the diurnal variations of PWV time series, an important climate signal, is obtained and analysed at a specific station (PIMO) during the El Niño event of 2014–2016 in Section 4. Section 5 gives the conclusion.

2. GPS ZTD data and accuracy analysis

The troposphere parameters derived from GPS observation have been found useful in meteorology to determine the atmospheric water vapour content (Bevis et al., 1992). In 1993, the IGS was established by the International Association of Geodesy and first released their related products on 1 January, 1994. In order to overcome the inhomogeneous of IGS-derived products, we selected the ZTD time series from “IGSnew” product provided by IGS. The “IGSnew” ZTD product is the new ZTD product which is provided after November 4, 2006 and the sampling interval is 5 min. This product is available from the beginning year of 2000 for all IGS stations and processed based on GIPSY PPP software using the IGS final orbits/clocks with an accuracy of better than 7 mm (Byun et al., 2005; Humphreys et al., 2005; Byun and Bar-Sever, 2009; Kouba, 2015). In the following subsections, due to the fixation of station location as well as the integrity of the selected data, only 4 collocated stations are selected between GPS and VLBI, 94 collocated stations are selected between GPS and radiosonde and 269 collocated stations are selected between GPS and GGOS atmosphere, respectively.

2.1. Comparison with VLBI

To validate the long time-series of ZTD products provided by the IGS, some comparisons are first performed. In our study, the ZTD derived from an independent technique –VLBI is first used to validate the accuracy of IGS ZTD products. The corresponding VLBI ZTD products can be downloaded for free from the independent Data Center of the International VLBI Service (IVS) (ftp://cddis.gsfc.nasa.gov/vlbi/ivsproducts/), which is a combined product offered by the IGG AC (Institute of Geodesy and Geophysics, Vienna University of Technology, Austria) after the Analysis Centres (ACs) of IVS have processed all available VLBI observations. Some studies have proved that the VLBI technique can provide reliable ZTD values with a high accuracy (Jin and Luo, 2009; Niell et al., 2001; Behrend et al., 2000; Snajdrova et al., 2006). However, the above studies only used a short-term VLBI ZTD product to validate the IGS ZTD products, i.e., with about two weeks of

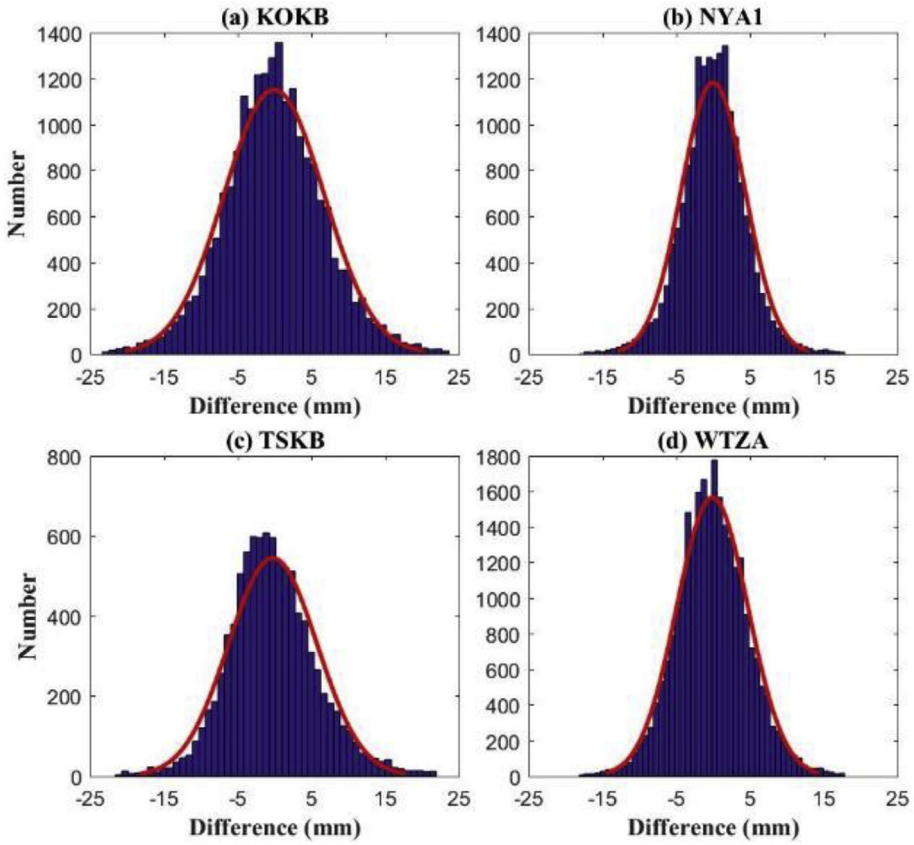

Fig. 2. Histogram of GPS-derived and VLBI-derived ZTD differences at four collocated stations, (a) KOKB, (b) NYA1, (c) TSKB and (d) WTZA over the period of 2002–2015.

data (Niell et al., 2001; Behrend et al., 2000; Snajdrova et al., 2006). In our study, a long-term VLBI ZTD time series of more than ten years (2002–2015) derived from independent Data Centres of IVS was selected to validate the accuracy of IGS ZTD products.

Four collocated stations between IGS and VLBI are selected according to the following principle: the horizontal distance between the VLBI station and IGS station must be less than 10 km and the vertical difference in their elevations must be less than 20 m. The time span of the selected ZTD time series is 14 years from 2002 to 2015 and the time interval is 1 h. A quality control procedure is performed before the comparison and it is based on the differences between the ZTD values obtained from IGS and IVS Data Centres. The ZTD values with differences larger than 3σ (standard deviation) are regarded as outliers. According to the analysis, about 0.84%, 1.28%, 1.38%, and 1.14% of ZTD data are rejected for four stations KOKB (USA), NYA1 (Norway), TSKB (Japan), and WTZA (Germany), respectively. Fig. 1 shows the comparison of GPS-derived and VLBI-derived ZTD at four collocated stations while Fig. 2 gives the error distribution histogram between GPS-derived and VLBI-derived ZTD at four collocated stations.

The statistical comparison of IGS ZTD and VLBI ZTD, including rejection rate, vertical differences and RMS error (the VLBI-derived ZTD is considered as a reference) is summarised in Table 1. It can be seen from Table 1 that the RMS error of IGS ZTD products is 6.8 mm, 4.3 mm, 6.0 mm and 4.8 mm for the four selected stations, respectively and the mean RMS error is about 5.5 mm. For the KOKB and TSKB stations, the RMS error is slightly larger than those at stations NYA1 and WTZA: the possible reasons may be that, (i) it is likely a latitudinal dependency (see Table 1), the RMS error decreased with the latitude increases for the selected 4 stations; (ii) the vertical elevation differences between the collocated stations of KOKB (9.0 m) and TSKB (14.8 m) are relatively larger than stations of NYA1 (3.3 m) and WTZA (3.4 m).

Table 1
Comparison result of ZTD time series derived from IGS and IVS at four collocated stations over the period of 2002–2016.

Collocated Station	Latitude (°)	Rejection Rate (%)	Vertical Difference (m)	RMS (mm)
KOKB	22.127	0.84	9.0	6.8
TSKB	36.103	1.38	14.8	6.0
WTZA	49.145	1.14	3.3	4.8
NYA1	78.928	1.28	3.4	4.3

2.2. Comparison with radiosonde data

Due to the lack of more collocated stations, another independent technique (Radio-sounding) is introduced to evaluate the accuracy of IGS ZTD products. Here, the radiosonde data derived from the Integrated Global Radiosonde Archive (IGRA) Version 2, which is produced by the National Climate Data Center (NCDC) and updated in August, 2016, is used. Compared to the IGRA 1, IGRA 2 provides more data (nearly as twice as many stations and 30% more soundings), longer records, more data sources (expect from fixed ground-based stations, data is also made available from floating stations and Russian ice-islands), additional variables are available, etc. More than 2000 globally distributed radiosonde stations from the earliest established in 1905 to those of the present day can be derived from the IGRA 2, which includes one to four sounding events daily. The corresponding dataset derived from IGRA 2 contains geopotential height, pressure, water vapour pressure, temperature, relative humidity, wind direction, wind speed, etc. All those parameters can be downloaded for free from the corresponding FTP ww-site (on-line at ftp://ftp.ncdc.noaa.gov/pub/data/igra/).

As for the quality of radiosonde data, a series of rigorous quality-

checking steps have been used to generate a comprehensive dataset before released. The vertical resolution of the sounding events has improved substantially with the average sounding containing 20 primary, and significant additional levels over the years (Wang et al., 2007; Ho et al., 2010; Durre et al., 2006). Wang et al. (2005, 2007) have analysed the sensitivity of PWV to missing radiosonde data above a specific pressure level and pointed out that only 0.61% of hydrostatic bias is introduced in PWV data if the data above 300 hPa pressure altitude are missing. Therefore, the radiosonde data with temperature and humidity profiles reaching at least 300 hPa are required in our study.

In our experiment, 94 collocated stations between IGS and radiosonde are selected on a global scale for the period 2005–2016. Although radiosonde sounding refers to a point observation, it measures the average values across a finite volume in the atmosphere (Kuo et al., 2005). Radiosonde balloons may drift horizontally by of tens of kilometres after launch (Ho et al., 2010). Seidel et al. (2011) proved that the mean drift distances of radiosonde balloons horizontally in upper troposphere and lower stratosphere are < 20 km and < 50 km, respectively, based on the 94 radiosonde stations on a global scale over the period from July, 2007 to July, 2009. Therefore, a criterion is determined in this paper such that the horizontal distance is less than 30 km while the vertical elevation difference is less than 100 m. Fig. 3 shows the Distribution of the RMS error and Bias of IGS ZTD products at 94 collocated stations when the radiosonde-derived ZTD is regarded as a reference. Statistical analysis reveals that the maximum/minimum/mean RMS errors and Bias are 18.7/8.7/17 mm and 10.7/-6.9/1.1 mm, respectively, while the rejected data was about 12.11%.

2.3. Comparison with GGOS atmosphere

In addition, the ZTD products for the IGS stations derived from GGOS Atmosphere, which is estimated and interpolated based on the ECMWF ERA-Interim data, are also compared with the IGS ZTD products. Here, 269 IGS stations for the period of 2005–2016 are selected and the sampling rate of ZTD products was set to 6 h in this study. Fig. 4 shows the distribution of the RMS error and Bias of ZTD differences between IGS-derived and GGOS-derived ZTD at 269 collocated stations. It can be seen from the Fig. 4 that the values of RMS error and Bias are increased with latitude decreases. The main reason for this is that the ZTD derived from GGOS Atmosphere is calculated from a numerical prediction model, which is not accurate when the water vapour content is high in low latitude areas. Statistical analysis shows that the maximum/minimum/mean RMS errors and Bias are 27/5/13 mm and 19/-9.6/2.5 mm, respectively.

3. Theoretical error analysis and PWV comparison

3.1. Error analysis of converting ZTD into PWV

PWV (in mm, equivalent to the Integrated Water Vapour content, IWV in kg/m^2) is the total water vapour content in the air column of unit area from the earth's surface to the top of the troposphere, which can be converted from ZWD and expressed as (Askne and Nordius, 1987):

$$\mathrm{PWV} = \Pi \cdot \mathrm{ZWD} \tag{1}$$

Where Π is a conversion factor, which can be expressed as:

$$\Pi = \frac{10^6}{\rho_w \cdot R_v \left[\frac{k_3}{T_m} + k_2'\right]} \tag{2}$$

Where ρ_w is the density of liquid water (unit: kg/m^3), R_v is the specific gas constant of water vapour (461.495 J/kg/K). k_2' and k_3 are constants with values of 22.1 ± 2.2 K/mb and 3.739 × 10^5 K^2/mb, respectively. T_m is the water-vapour-weighted mean temperature (unit: K), which can be calculated using the formula (Davis et al., 1985):

$$\mathrm{T_m} = \frac{\int \frac{P_w}{T} dh}{\int \frac{P_w}{T^2} dh} = \frac{\sum_1^n \left(\overline{\frac{P_{wi}}{T_i}}\right)(\mathrm{h_i} - \mathrm{h_{i-1}})}{\sum_1^n \left(\overline{\frac{P_{wi}}{T_i^2}}\right)(\mathrm{h_i} - \mathrm{h_{i-1}})} \tag{3}$$

Where P_w is the partial pressure of water vapour (unit: hPa) while T is the atmospheric temperature (unit: K). i is the ith pressure level and h_i is the corresponding height.

ZWD is the zenith wet delay, which can be extracted from ZTD by using the formula ZWD = ZTD−ZHD, where ZHD is the zenith hydrostatic delay, which can be expressed as (Saastamoinen, 1972):

$$\mathrm{ZHD} = \frac{0.002277 \cdot P_s}{1 - 0.00266 \cdot \cos(2\varphi) - 0.00028 \cdot H} \tag{4}$$

Where P_s is the surface pressure (unit: hPa), φ and H are the latitude and geodetic height of the station with the units of rad and km, respectively.

According to Eqs. (1) and (2), the relationship between the error of calculated PWV and errors in ZTD and $\mathrm{T_m}$ can be expressed by taking the derivative with respect to the ZWD and T_m. The following equations can be expressed how the errors in T_m and ZWD affect PWV:

$$\begin{aligned} \sigma_{\mathrm{pwv}} &= \Pi \cdot \sigma_{\mathrm{ZWD}} + \mathrm{ZWD} \cdot \sigma_{\Pi} \\ \sigma_{\Pi} &= \frac{10^6 \cdot k_3}{\rho_w \cdot R_v (k_3 + k_2' \cdot T_m)^2} \cdot \sigma_{T_m} \end{aligned} \tag{5}$$

Where σ_{pwv}, σ_{ZWD}, σ_{Π} and σ_{T_m} are the errors from PWV, ZWD, Π and T_m, separately. If Π and T_m take their average values of 0.15 and 281 K,

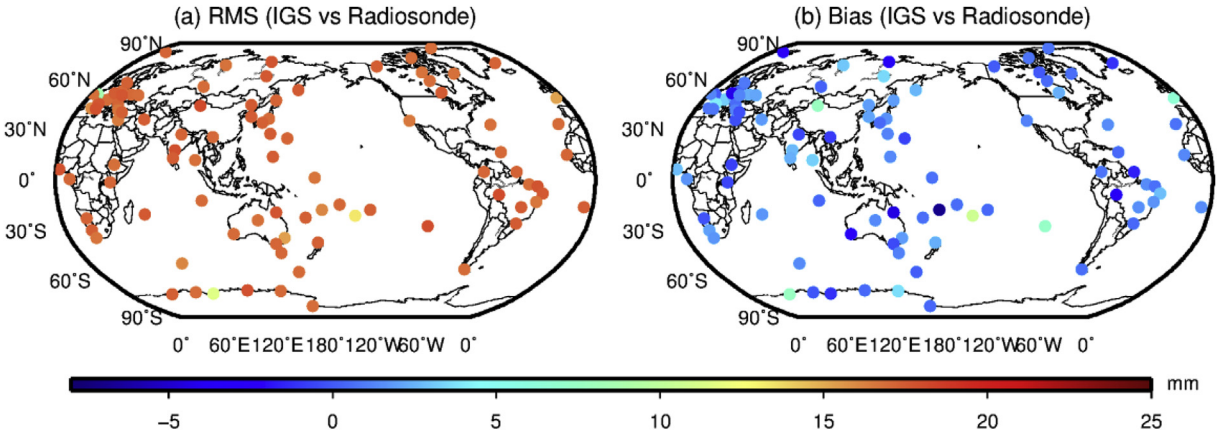

Fig. 3. Distribution of (a) RMS error and (b) Bias of ZTD differences between IGS-derived and Radiosonde-derived ZTD at 94 collocated stations over the period of 2005–2016.

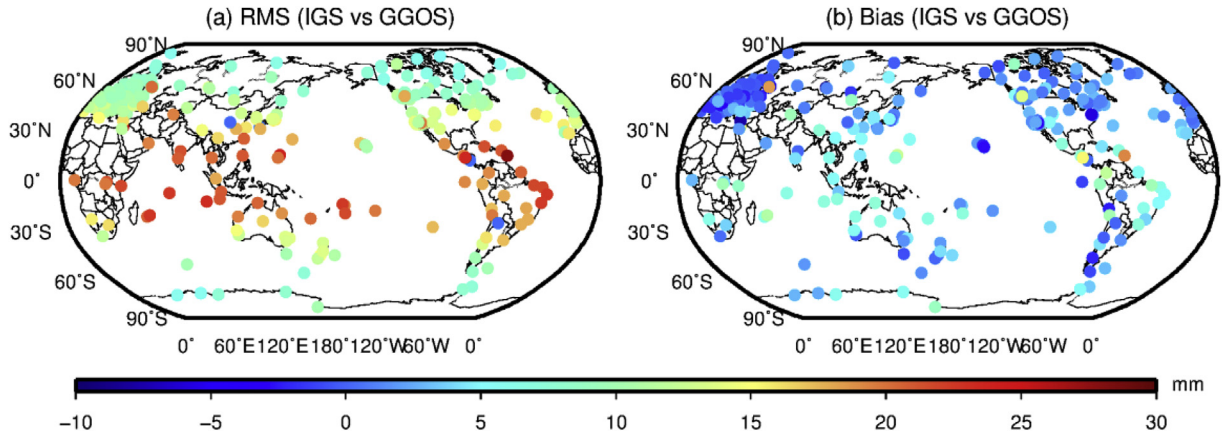

Fig. 4. Distribution of (a) the RMS error and (b) Bias of ZTD differences between IGS-derived and GGOS-derived ZTD at 269 collocated stations over the period of 2005–2016.

respectively, then, the Eq. (5) can be further simplified to:

$$\sigma_{\mathrm{pwv}} = 0.15\cdot\sigma_{\mathrm{ZWD}} + 5.6060\times10^{-4}\cdot\mathrm{ZWD}\cdot\sigma_{T_m}$$
$$\sigma_{\Pi} = 5.6060\times10^{-4}\cdot\sigma_{T_m}$$
$$\sigma_{\mathrm{ZWD}} = \sigma_{\mathrm{ZTD}} + \sigma_{\mathrm{ZHD}} \quad (6)$$

It can be seen from the second formula in the set of Eq. (6) that the error caused by T_m can be ignored and the second part of the first formula in the set of Eq. (6) is less than 1 mm. The error in σ_{ZHD} caused by 1 hPa change in P_s is about 2–3 mm ZHD error (Saastamoinen, 1972; Tregoning and Herring, 2006). In this paper, the P_s derived from GGOS has been validated with the RMS values less than 1 hPa when compared with the observes meteorological data (see Section 3.2) while the error in σ_{ZTD} is about 5–7 mm. Therefore, the error of σ_{ZWD} in the third formula of Eq. (6) is about 7–10 mm. According to the first formula of Eq. (6), the estimated error of PWV caused by errors in ZTD and ZHD is approximately 1–1.5 mm.

3.2. Accuracy validation of GGOS-derived P_s and T_m

As described in Section 3.1, the ZHD can be precisely calculated (Askne and Nordius, 1987; Saastamoinen, 1972; Elgered et al., 1991) using the surface pressure while Π is closely related to the temperature and atmospheric water vapour, which can be described as a function of weighted mean temperature of the atmosphere T_m (Bevis et al., 1992, 1994; Elgered et al., 1991). Therefore, the PWV derivation from ZWD is dependent only to two parameters: P_s and T_m.

In our study, the P_s and T_m data at all the IGS stations has been provided by GGOS Atmosphere, which should be validated before use. The GGOS-derived surface pressure is first compared with the surface pressure measured by the appropriately equipped meteorological sensors for 29 IGS stations globally over the period of 2005–2016. Currently, more than 70 IGS ground-based GPS stations are equipped with the meteorological sensors, which provide the meteorological data such as pressure, relative humidity, dew point temperature, etc. However, the data derived from meteorological sensors suffer from the occasional instances of poor data quality, noise and omissions. The sampling rate of surface pressure data is once every 2 h. Due to the surface pressure being provided by GGOS Atmosphere at UTC 00:00 06:00, 12:00, and 18:00, respectively, linear interpolation is used to find values at other times. Here, the differences of surface pressure from GGOS-meteorological data and GGOS-radiosonde data larger than 3σ (standard deviation) are regarded as outliers and rejected.

Fig. 5 (a) and (c) show the distribution of RMS error and Bias of surface pressure differences derived from GGOS Atmosphere and meteorological stations. Table 2 lists the RMS error of selected data, as well as the rejection rate applied to the meteorological data. Statistical result reveals that the maximum/minimum/mean RMS error and Bias of surface pressure differences are 1.8/0.1/0.8 hPa and 1.8/-0.8/0.4 hPa respectively, while the average rejection rate of meteorological data is only about 0.77%.

When comparing the measured surface pressures, GGOS-derived surface pressure is also compared with that from radiosonde at 78 collocated stations over the period 2005–2016. Fig. 5 (b) and (d) show the distribution of the RMS error and Bias of surface pressure differences derived from GGOS Atmosphere and radiosonde stations. Statistical analysis reveals that the maximum/minimum/mean RMS errors and Bias in surface pressure differences are 2.1/1.6/1.7 hPa and 1.1/-1.3/-0.2 hPa, respectively, while the average rejected data was about 21.6%. The relative large rejected data is existed because the collocated stations between GPS and radiosonde are not completely at the same location. As presented in Fig. 5 and Table 2, the RMS error and Bias of pressure differences between GGOS and meteorological stations are much smaller than that between GGOS and radiosonde stations. The mainly reason is also that the locations for GGOS and meteorological stations are totally collocated while a distance existed between GGOS and radiosonde stations.

In addition, GGOS-derived T_m is also compared with that from radiosonde data at 96 collocated stations for the period of 2005–2016. Fig. 6 shows the distribution of the RMS error and Bias of T_m when the radiosonde-derived T_m is regarded as a reference. Statistical analysis reveals that the maximum/minimum/mean RMS errors and Bias of temperature difference are 3.9/0.5/3.1 K and 3.9/-2.4/0.3 K, respectively, while the average rejected data was about 18.8%. Akilan et al. (2015) has been proved that the PWV error is less than 1 mm while the Tm error is 4 K, therefore, the error of Tm derived from GGOS can be neglected during the calculation of PWV.

3.3. Uniformity of height datum

Before comparing the meteorological parameters (P_s and T_m) derived from GGOS Atmosphere with that from radiosonde data, a procedure is required to unify the different heights to the same height system. For example, radiosonde data provides geopotential heights while the GGOS Atmosphere corresponds to ellipsoidal heights. In our study, the geopotential height is converted to geoid height.

(1) According to the relationship between geopotential height and geoid height proposed by Mahoney based on the WGS-84 geoid (Mahoney, 2008; Dousa and Elias, 2014; Zus et al., 2014; Wang et al., 2016), the geoid height can be calculated from geopotential height using the following formula:

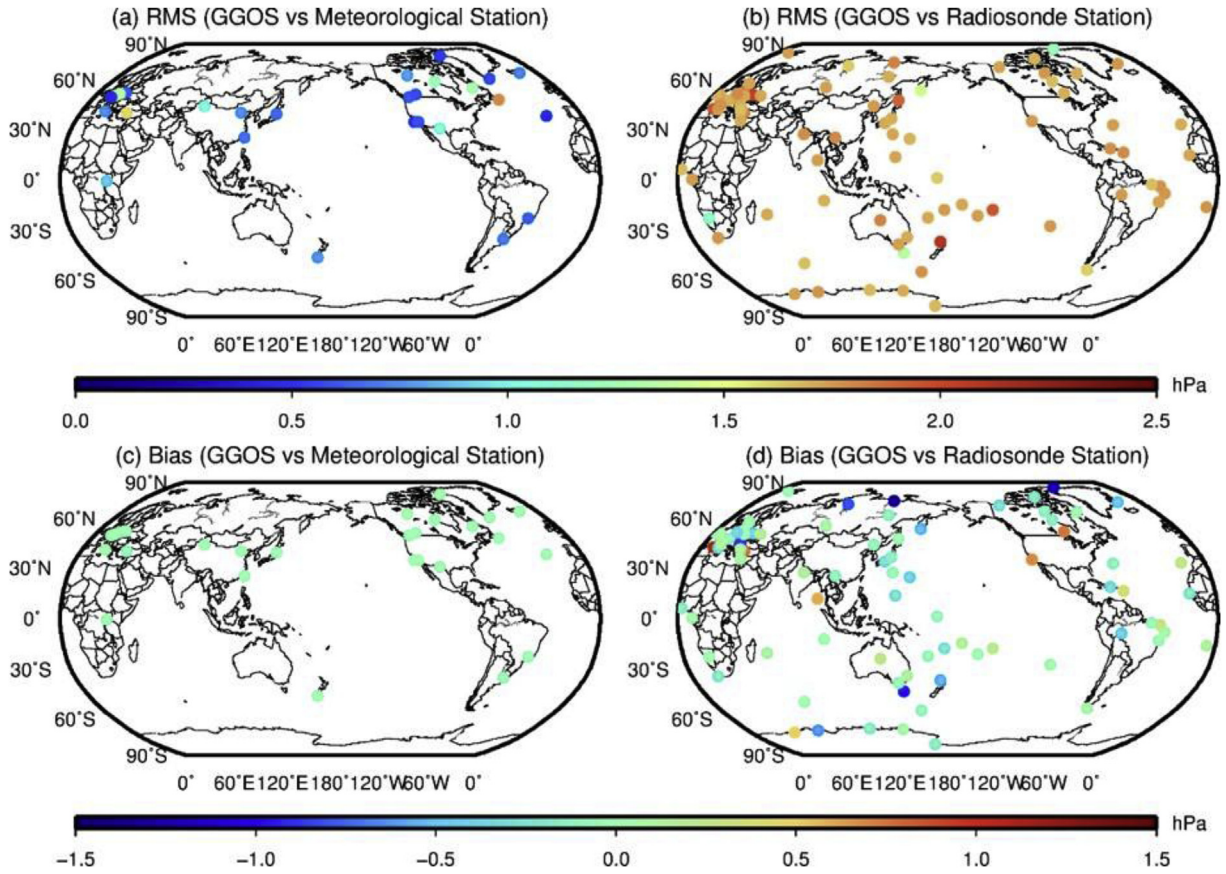

Fig. 5. Distribution of the RMS error and Bias of surface pressure differences between the GGOS-meteorological and GGOS-radiosonde stations at the collocated stations, where (a) and (b) represent the RMS error distribution while (b) and (d) refer to the Bias distribution, respectively over the period of 2005–2016.

$$GH(GPH,\varphi) = \frac{R(\varphi)\cdot Y_{45}\cdot GPH}{Y_S(\varphi)\cdot R(\varphi) - Y_{45}\cdot GPH}$$
$$Y_S(\varphi) = 9.780325\cdot\left[\frac{1+0.00193185\cdot\sin(\varphi)^2}{1-0.00669435\cdot\sin(\varphi)^2}\right]^{0.5}$$
$$R(\varphi) = \frac{6378.137}{1.006803 - 0.006706\cdot\sin(\varphi)^2} \quad (7)$$

Where GH is the geoid height. Y_{45} represents the normal acceleration due to gravity on the surface of the ellipsoid for latitude 45° with a value of 9.80665 m/s^2. R is an effective radius of the earth for latitude φ while Y_S is the normal gravitational acceleration on the surface of the ellipsoid of revolution.

(2) As for the conversion from WGS-84 ellipsoidal height, which is widely applied in GPS to geoid height, it can be realised by adopting the official Earth Gravitational Model 2008 (EGM2008) released by the U.S. National Geospatial-Intelligence Agency EGM Development Team (Vedel, 2000; Pavlis et al., 2008, 2012; Wang et al., 2016).

Meteorological parameters have been first converted to a unified elevation system. An interpolation procedure is then inevitable to obtain the meteorological parameters from radiosonde data for the location of GPS stations (Hagemann et al., 2003; Wang et al., 2005). Two types of interpolation are required, the first is vertical interpolation (extrapolation) for the meteorological parameters of selected stations. If the geoid height of a radiosonde station is lower than the corresponding height of the GPS station, linear interpolation is used based on the vertical difference in the two adjacent levels. Otherwise, vertical extrapolation is applied and the two methods can be used for the interpolation of temperature, which considers the mean lapse rates of temperature as a constant with a value of −6.5 K/km, or this mean lapse rate is calculated using the data from the lowest three model levels (Hagemann et al., 2003; Wang et al., 2005). Wang et al. (2016) find that the mean lapse rate is sometimes larger than 10 K/km or even

Table 2
RMS error of selected information and the rejection rate of meteorological data.

Station	Rejection Rate (%)	RMS (hPa)	Station	Rejection Rate (%)	RMS (hPa)	Station	Rejection Rate (%)	RMS (hPa)
ANKR	0.71	1.60	JOZE	0.86	0.61	QAQ1	1.47	0.55
BJFS	0.69	0.74	JPLM	1.00	0.58	SCH2	0.17	1.28
CHPI	0.83	0.61	LPGS	1.39	0.69	STJO	0.09	1.79
CHUR	0.32	1.23	MATE	2.15	0.73	THU2	1.26	0.54
DRAO	1.02	0.61	MBAR	0.13	0.88	THU3	1.29	0.53
GOPE	0.08	1.32	MDO1	0.10	1.07	TWTF	0.50	0.66
GUAO	0.60	1.07	MIZU	0.82	0.65	WROC	0.45	1.35
HARV	0.72	0.45	OUS2	1.00	0.74	WTZR	0.49	0.45
HOFN	0.95	0.70	PDEL	0.96	0.45	YELL	0.21	0.77
JOZ2	1.11	0.58	PRDS	0.96	0.57			

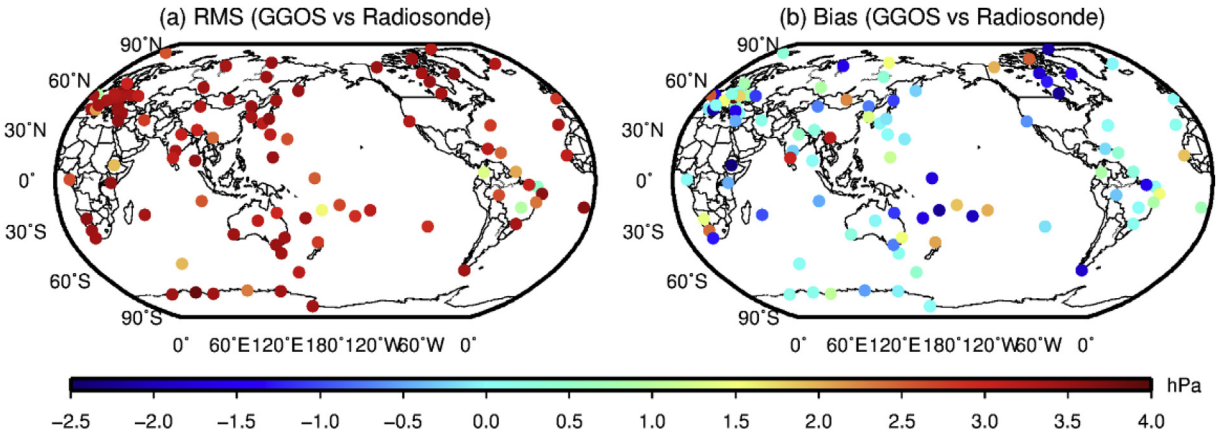

Fig. 6. Distribution of (a) RMS error and (b) Bias of T_m differences between GGOS and Radiosonde globally at 96 collocated stations over the period of 2005–2016.

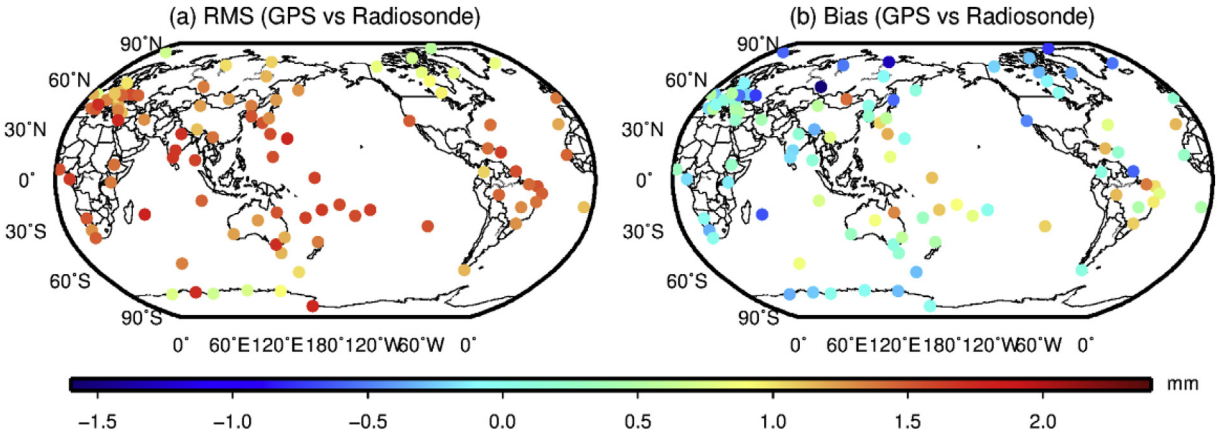

Fig. 7. Distribution of (a) RMS error and (b) Bias of PWV difference between GPS-derived and Radiosonde-derived PWV at 97 collocated stations over the period of 2005–2016.

Table 3
Geographical information of selected stations.

Station	ANKR	TDI1	SPT0	NKLG	BJFS	PIN1
Latitude (°)	29.89	−35.40	57.71	0.35	39.61	33.61
Longitude (°)	32.76	148.98	12.89	9.67	115.89	243.54
Height (m)	947.80	665.40	219.90	207.10	87.40	1256.20

negative, which could result in a large erroneous extrapolated temperature. Therefore, the mean lapse rate with a value of −6.5 K/km is used in our study which has been proved to be a favourable approximation to the tropospheric mean lapse rate in moist adiabatic conditions (Yang and Smith, 1985; Wang et al., 2005). The other meteorological parameters are extrapolated based on the mean lapse rates calculated using the data from the lowest three model levels.

3.4. PWV comparison

Although the ZTD product used in this paper is processed using the coherent strategy and its accuracy is about 1.9 mm (Byun and Bar-Sever, 2009; Kouba, 2015), a quality-control procedure is required before using this product, which is because the obtained ZTD in a long time series exist some problems like (i) the hardware changes (receivers, antennas, antennas radome type etc.); (ii) a lack of consistency due to some changes in GPS data-handling in elevation angle masks and antenna phase center variations (PCV) models by some/several data Analysis Centres (ACs); (iii) the improvement of the ZTD estimation algorithms arising from the introduction of new constraint schemes on the parameter estimation or mapping functions (Wang et al., 2007; Byun and Bar-Sever, 2009; Ning et al., 2016). In our study, the monthly mean and standard deviation (SD) of PWV time series are calculated at all stations and the values of PWV differences greater than 3σ are considered as outliers and rejected.

Based on the method introduced above for estimating PWV using P_s and T_m derived from GGOS Atmosphere, the 2-hourly IGS GPS-derived PWV are obtained on a global scale and compared with the PWV dataset calculated from radiosonde data. In the comparison of the PWV dataset for the period of 2005–2016, 97 collocated stations on a global scale are determined based on the principle that the horizontal differences between GPS and radiosonde stations are less than 30 km and elevation differences are less than 100 m, respectively. Fig. 7 shows the distribution of RMS error and Bias of PWV differences derived from GPS and radiosonde data at 97 collocated stations. It can be seen from Fig. 7 (a) that the RMS error of PWV difference is increased with latitude decreases, which is mainly caused by the fact that the water vapour content is large and the atmosphere activity is more active in low latitude areas. Therefore, the PWV error is relative large at low latitudes. Additionally, it also can be found from the Fig. 7 (b) that the Bias of PWV differences between GPS-derived and Radiosonde-derived are relative large at the areas of low latitudes while the values are small in polar regions, which is consistent with the result of RMS variations. Statistical analysis shows that the maximum/minimum/mean RMS errors and Bias are 1.8/0.6/1.3 mm and −1.55/1.43/0.21 mm, respectively, while the average rejected data was about 3.2%.

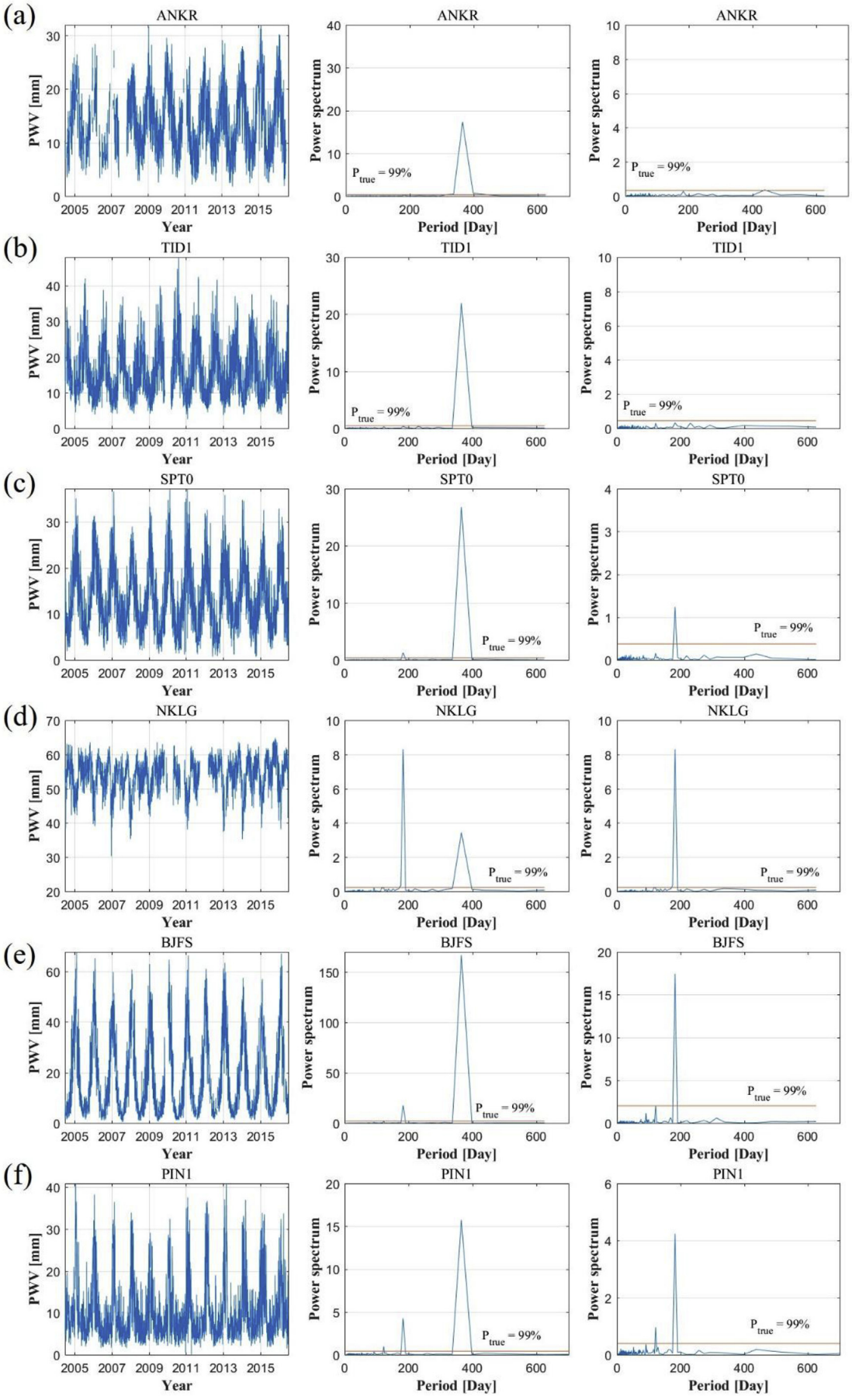

(caption on next page)

Fig. 8. Lomb-Scargle periodograms for stations (a) AJAC, (b) TID1, (c) SPT0, (d) NKLG, (e) BJFS and (f) PIN1, respectively over the period of 2005–2016. The first column represents the PWV time series while the second and third columns refer to the annual and semi-annual periods, respectively.

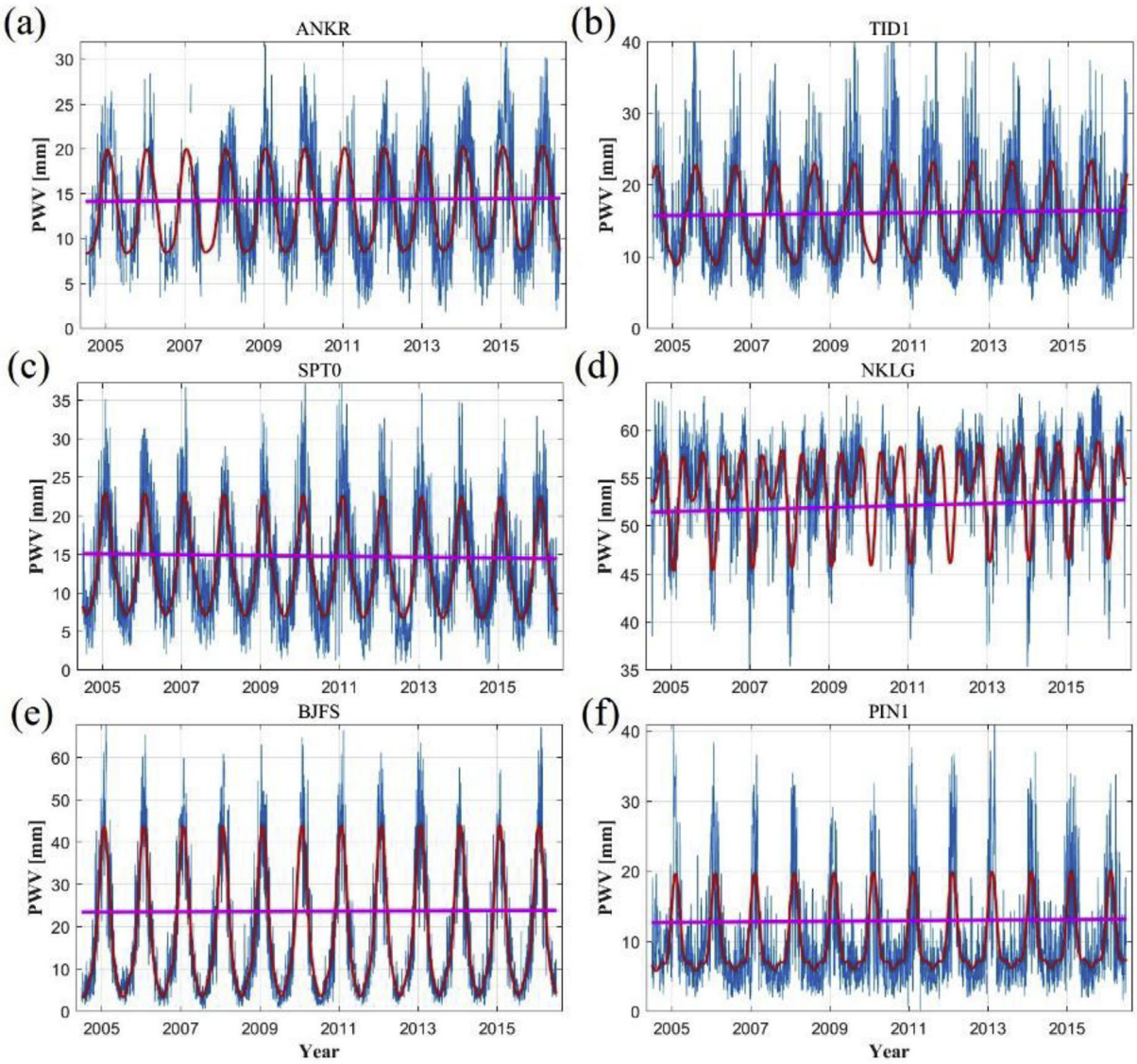

Fig. 9. PWV time series for six stations with fitted oscillations while the pink line represents the linear trend over the period of 2005–2016. (For interpretation of the references to colour in this figure legend, the reader is referred to the Web version of this article.)

4. Analysis of PWV time series

4.1. Annual, semi-annual and seasonal oscillations

PWV is a key parameter used to reflect the atmospheric water vapour variation with high spatio-temporal resolution. It changes depending on seasons, topography and regional climatic conditions. In this study, the 2-hourly GPS-derived PWV time series on a global scale is used to determine the values of seasonal variations as well as the linear trend in the PWV time series. However, one problem should be noted that the GPS-derived PWV time series is not equidistant, because of data gaps and rejected values from the GPS-derived ZTD data. To overcome this issue, the Lomb-Scargle periodogram method (Hocke, 1998) is introduced to detect the periodic components for data with some gaps. This periodogram is similar, but not identical, to classical Fourier spectrum analysis, which was originally proposed to solve the issues caused by uneven sampling or data with some gaps.

For the 199 IGS stations on the global scale, six stations (ANKR, TID1, SPT0, NKLG, BJFS and PIN1) are selected randomly and analysed their oscillations using the Lomb-Scargle periodogram method. The geographic information of the selected six stations has been presented in Table 3. Fig. 8 shows the results of six stations, where the first column shows the PWV time series over the period of 2005–2016, while the second and third columns list the power spectrum of PWV time series based on the Lomb-Scargle periodogram method. The difference between the second and third columns of Fig. 8 is that the third column removes the annual period. For stations AJAC and TID1 (Fig. 8 (a) and (b)), only annual oscillation exists with rejected data of 18.9% and 9.3%, respectively. For stations SPT0 and NKLG (Fig. 8 (c) and (d)), both annual and semi-annual oscillations exist with 1.4% and 19.2% of rejected data, respectively. In addition, the semi-annual oscillation of NKLG is larger than that of SPT0. For stations BJFS and PIN1 (Fig. 8 (e) and (f)), annual, semi-annual and seasonal oscillation exist with 10.8% and 4.6% of rejected data, respectively. By analysing all 199 selected

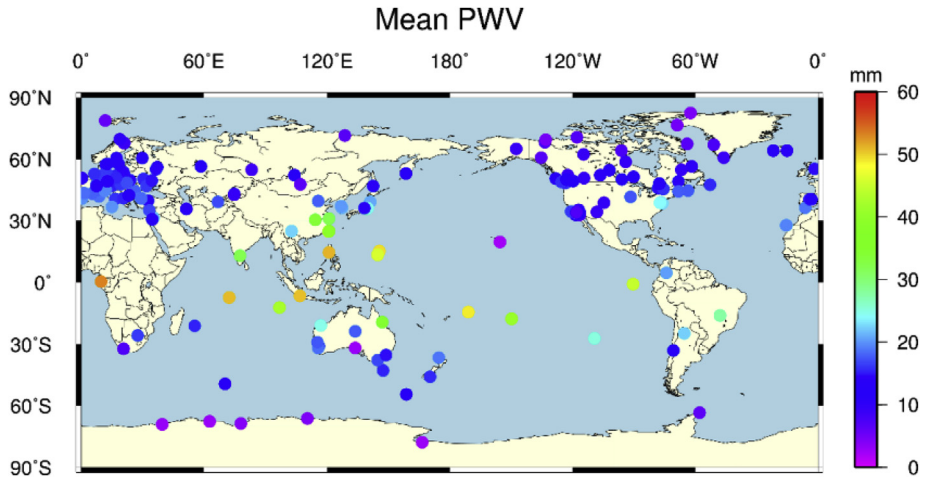

Fig. 10. Geographic distribution of the selected IGS stations globally and their mean PWV value.

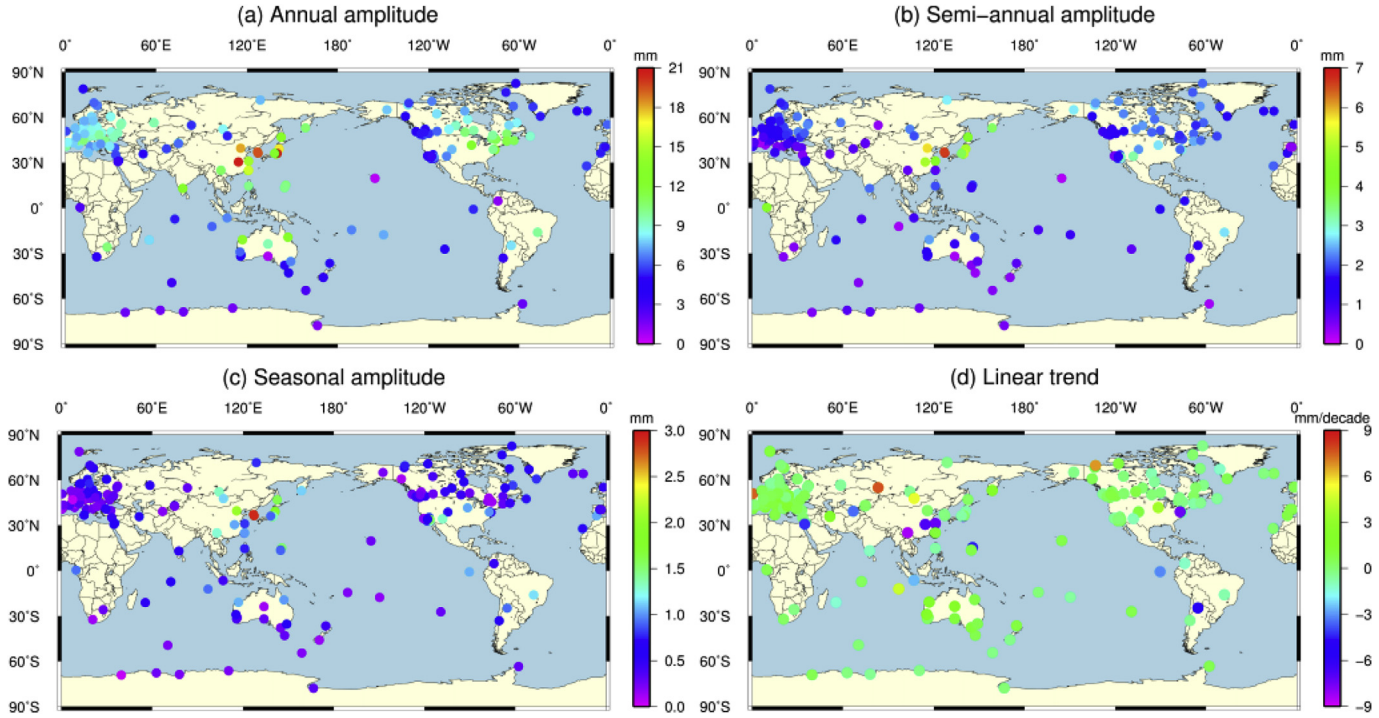

Fig. 11. Variations of (a) annual amplitude, (b) semi-annual amplitude, (c) seasonal amplitude and (d) linear trends for the selected IGS stations.

IGS PWV time series using the Lomb-Scargle periodogram method, we found that all stations exhibited a clear annual oscillation, most of them showed a semi-annual oscillation and some of them exhibited seasonal oscillations. Therefore, a linear least-squares sine and cosine model was introduced for the PWV time series:

$$x(t) = x_0 + v{\cdot}t + a_0{\cdot}\sin\left(2\pi\frac{t}{365.25}\right) + a_1{\cdot}\cos\left(2\pi\frac{t}{365.25}\right) + a_2{\cdot}\sin\left(4\pi\frac{t}{365.25}\right) + a_3{\cdot}\cos\left(4\pi\frac{t}{365.25}\right) + a_4{\cdot}\sin\left(6\pi\frac{t}{365.25}\right) + a_5{\cdot}\cos\left(6\pi\frac{t}{365.25}\right) \quad (8)$$

Where $x(t)$ is the PWV time series, x_0 is the mean value of PWV time series, v is the linear trend and $a_0 - a_5$ are coefficients of sine and cosine for annual, semi-annual and seasonal terms, respectively. The values of x_0, v and $a_0 - a_5$ are estimated based on the day-average values of the PWV dataset found using the least squares method.

Fig. 9 shows the corresponding PWV time series for six stations with fitted oscillations. It can be seen that the missing values in the PWV time series can be fitted based on the Lomb-Scargle periodogram method and the linear model proposed above. The sizes of linear trend, annual, semi-annual and seasonal amplitudes are various for different stations. Therefore, those terms are further analysed on a global scale by using data from the 199 IGS stations. Fig. 10 shows the mean PWV values at the selected 199 IGS stations. It can be concluded that the value of mean PWV increased with decreasing latitude and the maximum/minimum values of mean PWV are about 53.3 mm and 2.4 mm, respectively. Such phenomenon can be explained that the water vapour content is large at low latitudes. Fig. 11 shows the annual, semi-annual and seasonal amplitudes as well as the linear trends for 199 IGS stations. Fig. 11 (a) shows that the maximum value of annual amplitude occurs at station WUHN, China, with a value of 20.1 mm and the values are large in eastern China, Korea and Japan. From Fig. 11 (b) and (c), we can conclude that the maximum semi-annual and seasonal amplitudes occur at DAEJ and SUWN, Korea, with values of 6.8 mm and 2.9 mm, respectively. Fig. 11 (d) also shows the linear trend in IGS station data over a decade and most linear trend slopes of the selected

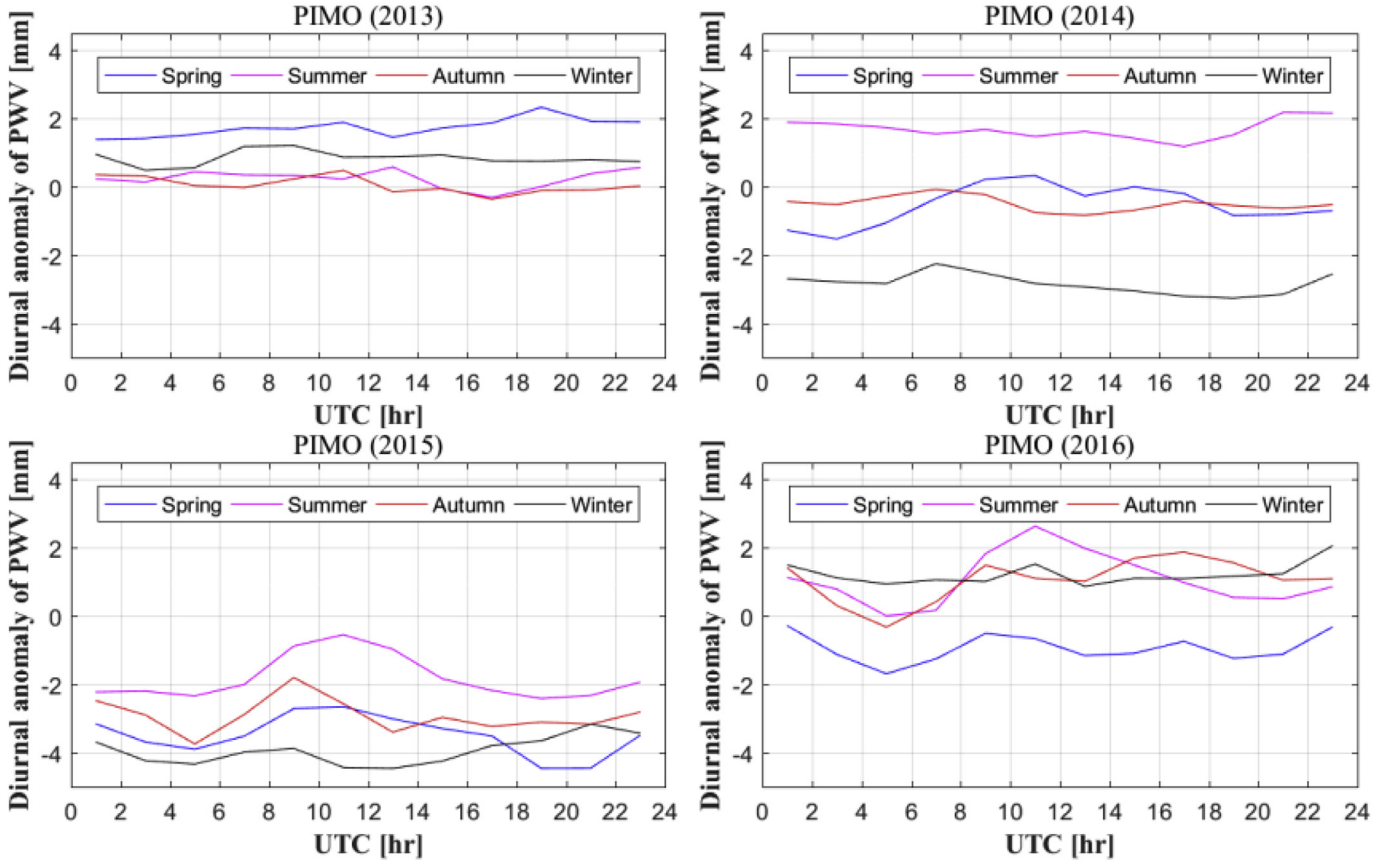

Fig. 12. Diurnal anomalies of PWV time series as a function of UTC at PIMO station.

IGS station data are positive with a value of 1–4 mm/decades. Additionally, it also can be found that the linear trend with an upward trend mainly existed in the areas of Europe, Australian and American.

4.2. PWV diurnal variations

The 2-hourly PWV data set obtained by the proposed method can be used to calculate the diurnal variation therein, which is an important indicator of climate signal. According to the meteorological custom, four seasons are described as follows: Spring from March to May, Summer from June to August, Autumn from September to November and Winter from December to February.

Seasonal mean diurnal anomalies for the period 2013–2016 are presented in station PIMO (Philippines), where is taken as an example for investigating diurnal PWV variations based on the estimated 2-hourly PWV dataset (see Fig. 12). The diurnal anomaly of PWV time series is obtained by removing the seasonal mean value in each day. It can be seen from Fig. 12 that the average water vapour content is decreased in 2014 except for Summer when compared to 2013, then, the values in all four seasons decreased in 2015 and then increased to different extents in 2016. The main reason for this trend in PWV diurnal anomalies is the El Niño event that started in 2014 and ended in 2016. El Niño events lead to global changes of climate and a drought was initiated in The Philippines, therefore, the PWV diurnal variation first decreases due to the drought happened over the period of 2014–2015, and then increased to its average level over period of 2015–2016. Statistical analysis of the results from station PIMO shows that the differences in PWV diurnal anomaly are −2.3/1.4/-0.5/-3.7 mm, −3.0/-3.5/-2.4/-1.1 mm and 2.6/2.9/4.0/5.2 mm for 2013–2014, 2014–2015 and 2015–2016, respectively.

5. Conclusion

A method of converting ZTD-derived data from the IGS GPS network to PWV on a global scale is proposed in this paper. The key parameters, ZTD, P_s, and T_m, are validated with different and independent techniques. The IGS-derived ZTD is evaluated globally using the VLBI-derived, and radiosonde-derived ZTD, respectively. The P_s data derived from GGOS Atmosphere is also compared with data from meteorological sensors as well as those from radiosonde recordings, respectively. Finally, the GPS-derived PWV time series can be obtained with the RMS error less than 1.5 mm by comparing that with the radiosonde data at 97 collocated stations on a global scale. It must be noted that the accuracy of ZTD is different when compared to VLBI (5.5 mm) and radiosonde data (17 mm). The large ZTD differences between GPS and radiosonde is caused by that the data from radiosonde stations is not strictly from the fixed point and time as described in section 2.2. The above reasons caused a relative large difference between GPS and radiosonde data.

The 12-year, 2-hourly GPS-derived PWV time series is analysed by the Lomb-Scargle periodogram method to detect different variations in 199 stations. By introducing the Lomb-Scargle periodogram method, the disadvantage of data gaps from PWV time series can be well-resolved. It has been shown, by analysing the mean PWV, that the water vapour at low latitudes was more abundant, while the lower-vapour contents were found in higher latitude areas. In addition, it can be concluded that the water vapour was more active in eastern China, Korea, and Japan according to the different amplitudes and linear trends observed while shows an upward trend in the areas of Europe, Australian and American. Additionally, one important climate signal, a diurnal cycle, is also calculated and analysed at station PIMO in Philippines, which shows something interesting during an El Niño event. The preliminary result from anomalies analysis of diurnal cycle

reveals the significant relationship between PWV time series and El Niño and their profound connotation needs the further study.

The PWV data obtained in this paper provides a new source of data for atmospheric water analysis with high-temporal resolution, long-term stability and at low cost. We expect that other researchers may use such data, which can be acquired from the authors upon request.

Acknowledgement

The author would like to thank IGS for providing highly precise GPS ZTD products, the GGOS Atmosphere, IVS Data Centres and IGRA are also thanked for providing the corresponding data. This research was supported by the Excellent Youth Science and Technology Fund Project of Xi'an University of Science and Technology (2018YQ3-12) and the Startup Foundation for Doctor of Xi'an University of Science and Technology (2017QDJ041).

References

Adams, D.K., Fernandes, R.M.S., Maia, J.M.F., 2011. GNSS precipitable water vapor from an Amazonian rain forest flux tower. J. Atmos. Ocean. Technol. 28, 1192–1198.
Akilan, A., Azeez, K.K.A., Balaji, S., Schuh, H., Srinivas, Y., 2015. GPS derived zenith total delay (ZTD) observed at tropical locations in south India during atmospheric storms and depressions. J. Atmos. Sol. Terr. Phys. 125–126, 1–7.
Askne, J., Nordius, H., 1987. Estimation of tropospheric delay for microwaves from surface weather data. Radio Sci. 22, 379–386.
Bałdysz, Z., Nykiel, G., Figurski, M., et al., 2015. Investigation of the 16-year and 18-year ZTD time series derived from GPS data processing. Acta Geophys. Pol. 6, 1103–1125.
Baldysz, Z., Nykiel, G., Figurski, M., et al., 2018. Assessment of the impact of GNSS processing strategies on the long-term parameters of 20 Years IWV time series. Rem. Sens. 10 (4), 496.
Basili, P., Bonafoni, S., Mattioli, V., et al., 2004. Mapping the atmospheric water vapor by integrating microwave radiometer and GPS measurements. IEEE Trans. Geosci. Rem. Sens. 42, 1657–1665.
Behrend, D., Cucurull, L., Vilà, J., et al., 2000. An inter-comparison study to estimate zenith wet delays using VLBI, GPS, and NWP models. Earth Planets Space 52, 691–694.
Bevis, M., Businger, S., Chiswell, S., et al., 1994. GPS meteorology: mapping zenith wet delays onto precipitable water. J. Appl. Meteorol. 33, 379–386.
Bevis, M., Businger, S., Herring, T.A., et al., 1992. GPS meteorology: remote sensing of atmospheric water vapor using the Global Positioning System. J. Geophys. Res. Atmos. 97, 15787–15801.
Byun, S.H., Bar-Sever, Y.E., 2009. A new type of troposphere zenith path delay product of the international GNSS service. J. Geodes. 83, 1–7.
Byun, S.H., Bar-Sever, Y., Gendt, G., 2005. The New Tropospheric Product of the International GNSS Service. Jet Propulsion Laboratory, National Aeronautics and Space Administration, Pasadena, CA.
Dai, A., Wang, J., Ware, R.H., et al., 2002. Diurnal variation in water vapor over North America and its implications for sampling errors in radiosonde humidity. J. Geophys. Res. Atmosphere 107 (D10).
Davis, J.L., Herring, T.A., Shapiro, I.I., et al., 1985. Geodesy by radio interferometry: effects of atmospheric modeling errors on estimates of baseline length. Radio Sci. 20, 1593–1607.
Dousa, J., Elias, M., 2014. An improved model for calculating tropospheric wet delay. Geophys. Res. Lett. 41, 4389–4397.
Durre, I., Vose, R.S., Wuertz, D.B., 2006. Overview of the integrated global radiosonde archive. J. Clim. 19, 53–68.
Elgered, G., Davis, J.L., Herring, T.A., et al., 1991. Geodesy by radio Ingerferomery'Waer vapor radiomegry for estimation of delay. J. Geophys. Res. 96, 6541–6555.
Elgered, G., Johansson, J.M., Rönnäng, B.O., et al., 1997. Measuring regional atmospheric water vapor using the Swedish permanent GPS network. Geophys. Res. Lett. 24, 2663–2666.
Gaffen, D.J., Barnett, T.P., Elliott, W.P., 1991. Space and time scales of global tropospheric moisture. J. Clim. 4, 989–1008.
Gao, B.C., Chan, P.K., Li, R.R., 2004. A global water vapor data set obtained by merging the SSMI and MODIS data. Geophys. Res. Lett. 31 (18).
Grejner-Brzezinska, D.A., 2013. GPS-PWV estimation and validation with radiosonde data and numerical weather prediction model in Antarctica. GPS Solut. 17, 29–39.
Hagemann, S., Bengtsson, L., Gendt, G., 2003. On the determination of atmospheric water vapor from GPS measurements. J. Geophys. Res. Atmos. 108 (D21).
Hernández-Pajares, M., Juan, J.M., Sanz, J., et al., 2001. A new strategy for real-time integrated water vapor determination in WADGPS networks. Geophys. Res. Lett. 28, 3267–3270.
Ho, S.P., Zhou, X., Kuo, Y.H., et al., 2010. Global evaluation of radiosonde water vapor systematic biases using GPS radio occultation from COSMIC and ECMWF analysis. Rem. Sens. 2, 1320–1330.
Hocke, K., 1998. Phase estimation with the Lomb-Scargle periodogram method. Ann. Geophys. 16, 356–358.
Humphreys, T.E., Kelley, M.C., Huber, N., et al., 2005. The semidiurnal variation in GPS-derived zenith neutral delay. Geophys. Res. Lett. 32 (24).
Jin, S., Luo, O.F., 2009. Variability and climatology of PWV from global 13-year GPS observations. IEEE Trans. Geosci. Rem. Sens. 47, 1918–1924.
Jin, S., Park, J.U., Cho, J.H., et al., 2007. Seasonal variability of GPS-derived zenith tropospheric delay (1994–2006) and climate implications. J. Geophys. Res. Atmos. 112 (D9).
Kouba, J., 2015. A Guide to Using International GPS Service (IGS) Products. A Report Prepared for IGS. available at: ftp://igscb.jpl.nasa.gov/igscb/resource/pubs/GuidetoUsingIGSProducts.pdf.
Kuo, Y.H., Guo, Y.R., Westwater, E.R., 1993. Assimilation of precipitable water measurements into a mesoscale numerical model. Mon. Weather Rev. 121, 1215–1238.
Kuo, Y.H., Schreiner, W.S., Wang, J., Rossiter, D.L., et al., 2005. Comparison of GPS radio occultation soundings with radiosondes. Geophys. Res. Lett. 32 (5).
Mahoney, M.J., 2008. A Discussion of Various Measures of Altitude. Jet Propulsion Laboratory. http://mtp.jpl.nasa.gov/notes/altitude/altitude.Html.
Niell, A.E., Coster, A.J., Solheim, F.S., et al., 2001. Comparison of measurements of atmospheric wet delay by radiosonde, water vapor radiometer, GPS, and VLBI. J. Atmos. Ocean. Technol. 18, 830–850.
Nilsson, T., Gradinarsky, L., 2006. Water vapor tomography using GPS phase observations: simulation results. IEEE Trans. Geosci. Rem. Sens. 44, 2927–2941.
Ning, T., Wang, J., Elgered, G., et al., 2016. The uncertainty of the atmospheric integrated water vapour estimated from GNSS observations. Atmos. Meas. Tech. 9 (1), 79.
Pavlis, N.K., Holmes, S.A., Kenyon, S.C., et al., 2008. An earth gravitational model to degree 2160: EGM2008. EGU General Assembly 4, 13–18.
Pavlis, N.K., Holmes, S.A., Kenyon, S.C., et al., 2012. The development and evaluation of the earth gravitational model 2008 (EGM2008). J. Geophys. Res. B solid earth 117 (B4).
Ross, R.J., Elliott, W.P., 2001. Radiosonde-based Northern Hemisphere tropospheric water vapor trends. J. Clim. 14, 1602–1612.
Ross, R.J., Elliott, W.P., 1996. Tropospheric water vapor climatology and trends over North America: 1973–93. J. Clim. 9, 3561–3574.
Saastamoinen, J., 1972. Atmospheric Correction for the Troposphere and Stratosphere in Radio Ranging Satellites. The Use of Artificial Satellites for Geodesy. pp. 247–251.
Schueler, T., Pósfay, A., Hein, G.W., et al., 2001. A global analysis of the mean atmospheric temperature for GPS water vapor estimation. In: Proceedings of ION-GPS, pp. 11–14.
Seidel, D.J., Sun, B., Pettey, M., et al., 2011. Global radiosonde balloon drift statistics. J. Geophys. Res. Atmos. 116 (D7).
Snajdrova, K., Böhm, J., Willis, P., et al., 2006. Multi-technique comparison of tropospheric zenith delays derived during the CONT02 campaign. J. Geodes. 79, 613–623.
Tregoning, P., Boers, R., O'Brien, D., et al., 1998. Accuracy of absolute precipitable water vapor estimates from GPS observations. J. Geophys. Res. Atmos. 103, 28701–28710.
Tregoning, P., Herring, T.A., 2006. Impact of a priori zenith hydrostatic delay errors on GPS estimates of station heights and zenith total delays. Geophys. Res. Lett. 33 (23).
Trenberth, K.E., Fasullo, J., Smith, L., 2005. Trends and variability in column-integrated atmospheric water vapor. Clim. Dynam. 24, 741–758.
Vedel, H., 2000. Conversion of WGS84 Geometric Heights to NWP Model HIRLAM Geopotential Heights. Danish Meteorological Institute.
Wang, J., Zhang, L., Dai, A., 2005. Global estimates of water-vapor-weighted mean temperature of the atmosphere for GPS applications. J. Geophys. Res. Atmos. 110 (D21).
Wang, J., Zhang, L., Dai, A., et al., 2007. A near-global, 2-hourly data set of atmospheric precipitable water from ground-based GPS measurements. J. Geophys. Res. Atmos. 112 (D11).
Wang, X., Zhang, K., Wu, S., et al., 2016. Water vapor-weighted mean temperature and its impact on the determination of precipitable water vapor and its linear trend. J. Geophys. Res. Atmos. 121, 833–852.
Wu, P., Hamada, J.I., Mori, S., et al., 2003. Diurnal variation of precipitable water over a mountainous area of Sumatra Island. J. Appl. Meteorol. 42, 1107–1115.
Yang, S.K., Smith, G.L., 1985. Further study on atmospheric lapse rate regimes. J. Atmos. Sci. 42, 961–966.
Zus, F., Dick, G., Douša, J., et al., 2014. The rapid and precise computation of GPS slant total delays and mapping factors utilizing a numerical weather model. Radio Sci. 49, 207–216.